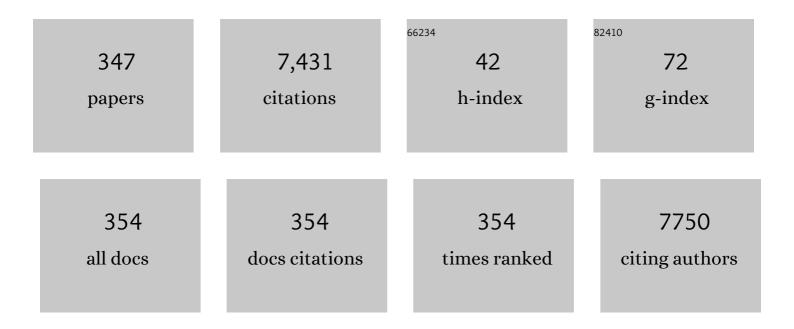
List of Publications by Year in descending order

Source: https://exaly.com/author-pdf/773848/publications.pdf Version: 2024-02-01



MARK AINDOW

#	Article	IF	CITATIONS
1	ZnO with Different Morphologies Synthesized by Solvothermal Methods for Enhanced Photocatalytic Activity. Chemistry of Materials, 2009, 21, 2875-2885.	3.2	444
2	Effect of self-accommodation on α/α boundary populations in pure titanium. Acta Materialia, 2003, 51, 2485-2503.	3.8	266
3	Synthesis and Catalytic Activity of Cryptomelane-Type Manganese Dioxide Nanomaterials Produced by a Novel Solvent-Free Method. Chemistry of Materials, 2005, 17, 5382-5389.	3.2	229
4	Hydrothermal Synthesis of Structure- and Shape-Controlled Manganese Oxide Octahedral Molecular Sieve Nanomaterials. Advanced Functional Materials, 2006, 16, 1247-1253.	7.8	212
5	Hydrothermal Growth of Manganese Dioxide into Three-Dimensional Hierarchical Nanoarchitectures. Advanced Functional Materials, 2006, 16, 549-555.	7.8	195
6	Effect of heat treatments on microstructural evolution of additively manufactured and wrought 17-4PH stainless steel. Materials and Design, 2018, 156, 429-440.	3.3	169
7	Control of Nanometer-Scale Tunnel Sizes of Porous Manganese Oxide Octahedral Molecular Sieve Nanomaterials. Advanced Materials, 2005, 17, 805-809.	11.1	159
8	Pseudo-elastic deformation behavior in a Ti/Mo-based alloy. Scripta Materialia, 2004, 50, 343-348.	2.6	121
9	Effects of Alkali Metal and Ammonium Cation Templates on Nanofibrous Cryptomelane-type Manganese Oxide Octahedral Molecular Sieves (OMS-2). Journal of Physical Chemistry B, 2003, 107, 9185-9194.	1.2	115
10	Preparation of Platinum/Carbon Aerogel Nanocomposites Using a Supercritical Deposition Method. Journal of Physical Chemistry B, 2004, 108, 7716-7722.	1.2	108
11	Investigation of the supercritical deposition of platinum nanoparticles into carbon aerogels. Microporous and Mesoporous Materials, 2005, 80, 11-23.	2.2	105
12	Supported Platinum Nanoparticles by Supercritical Deposition. Industrial & Engineering Chemistry Research, 2005, 44, 4161-4164.	1.8	101
13	Behavior of H2 chemisorption on Ru/TiO2 surface and its application in evaluation of Ru particle sizes compared with TEM and XRD analyses. Applied Catalysis A: General, 2008, 335, 187-195.	2.2	95
14	The mechanical properties and the deformation microstructures of the C15 Laves phase Cr2Nb at high temperatures. Acta Materialia, 2007, 55, 1873-1884.	3.8	88
15	In situ Synthesis of Mixed-Valent Manganese Oxide Nanocrystals:Â An In situ Synchrotron X-ray Diffraction Study. Journal of the American Chemical Society, 2006, 128, 4570-4571.	6.6	85
16	Grain growth and particle pinning in a model Ni-based superalloy. Materials Science & Engineering A: Structural Materials: Properties, Microstructure and Processing, 2008, 479, 365-372.	2.6	85
17	Facet-dependent catalytic activity of MnO electrocatalysts for oxygen reduction and oxygen evolution reactions. Chemical Communications, 2015, 51, 5951-5954.	2.2	84
18	Effects of low-power plasma treatment on polyethylene surfaces. Surface and Interface Analysis, 1995, 23, 319-327.	0.8	83

#	Article	IF	CITATIONS
19	Formation of spinel reaction layers in manganese cobaltite – coated Crofer22 APU for solid oxide fuel cell interconnects. Journal of Power Sources, 2013, 227, 318-326.	4.0	81
20	Amine-Assisted Facetted Etching of CdSe Nanocrystals. Journal of the American Chemical Society, 2005, 127, 2524-2532.	6.6	80
21	Preparation and Characterization of Ruthenium/Carbon Aerogel Nanocomposites via a Supercritical Fluid Route. Journal of Physical Chemistry B, 2005, 109, 2617-2624.	1.2	78
22	Size Control, Metal Substitution, and Catalytic Application of Cryptomelane Nanomaterials Prepared Using Cross-linking Reagents. Chemistry of Materials, 2004, 16, 276-285.	3.2	76
23	Non-metallic inclusions in 17-4PH stainless steel parts produced by selective laser melting. Materials and Design, 2018, 140, 153-162.	3.3	76
24	Interfacial dislocation mechanism for diffusional phase transformations exhibiting martensitic crystallography: formation of TiAl + Ti3Al lamellae. Acta Materialia, 2000, 48, 1047-1053.	3.8	70
25	Preparation of carbon black supported Pd, Pt and Pd–Pt nanoparticles using supercritical CO2 deposition. Journal of Supercritical Fluids, 2009, 50, 82-90.	1.6	70
26	Selective hydrogenation of CO2 and CO to useful light olefins over octahedral molecular sieve manganese oxide supported iron catalysts. Applied Catalysis B: Environmental, 2013, 132-133, 54-61.	10.8	70
27	Dielectric response and tunability of a dielectric-paraelectric composite. Applied Physics Letters, 2008, 93, 102908.	1.5	66
28	Pt-based electrocatalysts for polymer electrolyte membrane fuel cells prepared by supercritical deposition technique. Journal of Power Sources, 2008, 179, 532-540.	4.0	64
29	Synthesis, Characterization, and Catalytic Applications of Manganese Oxide Octahedral Molecular Sieve (OMS) Nanowires with a 2 × 3 Tunnel Structure. Chemistry of Materials, 2004, 16, 5327-5335.	3.2	57
30	Decoration of multi-wall carbon nanotubes with platinum nanoparticles using supercritical deposition with thermodynamic control of metal loading. Scripta Materialia, 2007, 56, 101-103.	2.6	57
31	Corrosion, oxidation, erosion and performance of Ag/W-based circuit breaker contacts: A review. Corrosion Science, 2018, 135, 12-34.	3.0	54
32	Nucleation of stress-induced martensites in a Ti/Mo-based alloy. Journal of Materials Science, 2005, 40, 2833-2836.	1.7	53
33	A study of surface cross-hatch and misfit dislocation structure in grown by chemical beam epitaxy. Journal of Crystal Growth, 1995, 149, 1-11.	0.7	52
34	Magnesium Manganese Oxide Nanoribbons:Â Synthesis, Characterization, and Catalytic Application. Journal of Physical Chemistry B, 2002, 106, 9761-9768.	1.2	52
35	Shape Evolution of Single-Crystalline Mn2O3Using a Solvothermal Approach. Journal of Physical Chemistry C, 2007, 111, 14694-14697.	1.5	52
36	The effect of recycling on the oxygen distribution in Ti-6Al-4V powder for additive manufacturing. Materials at High Temperatures, 2018, 35, 217-224.	0.5	52

#	Article	IF	CITATIONS
37	Adsorption of Pt(cod)me2 onto organic aerogels from supercritical solutions for the synthesis of supported platinum nanoparticles. Journal of Supercritical Fluids, 2011, 56, 105-113.	1.6	50
38	Graphene Aerogel Supported Pt Electrocatalysts for Oxygen Reduction Reaction by Supercritical Deposition. Electrochimica Acta, 2017, 250, 174-184.	2.6	50
39	Mesoscale modeling of jet initiation behavior and microstructural evolution during cold spray single particle impact. Acta Materialia, 2020, 182, 197-206.	3.8	48
40	Effects of alloy heat treatment on oxidation kinetics and scale morphology for Crofer 22 APU. Journal of Power Sources, 2013, 241, 756-767.	4.0	47
41	On the role of the pore filling medium in photoluminescence from photochemically etched porous silicon. Journal of Applied Physics, 2000, 88, 2472-2479.	1.1	46
42	The structure of ribbon borides in a Ti-44Al-4Nb-4Zr-1B alloy. Intermetallics, 2006, 14, 759-769.	1.8	46
43	Identification of Desirable Precursor Properties for Solution Precursor Plasma Spray. Journal of Thermal Spray Technology, 2011, 20, 802-816.	1.6	44
44	Dislocation processes during the plastic deformation of Î <sup>3</sup> -TiAl. Philosophical Magazine A: Physics of Condensed Matter, Structure, Defects and Mechanical Properties, 1999, 79, 1045-1071.	0.8	43
45	Phase stability and microstructure in devitrified Al-rich Al–Y–Ni alloys. Intermetallics, 2004, 12, 349-362.	1.8	42
46	Origin of pseudoelastic behavior in Ti–Mo-based alloys. Applied Physics Letters, 2005, 87, 241909.	1.5	42
47	PtPd/BP2000 electrocatalysts prepared by sequential supercritical carbon dioxide deposition. International Journal of Hydrogen Energy, 2010, 35, 11669-11680.	3.8	42
48	Preface to the 50th anniversary issue of the Journal of Materials Science. Journal of Materials Science, 2016, 51, 1-6.	1.7	41
49	Microstructures and mechanical properties of Nb–Ti–C alloys. Materials Science & Engineering A: Structural Materials: Properties, Microstructure and Processing, 2008, 485, 359-366.	2.6	40
50	Thermodynamic Control of Metal Loading and Composition of Carbon Aerogel Supported Pt–Cu Alloy Nanoparticles by Supercritical Deposition. Journal of Physical Chemistry C, 2013, 117, 6777-6787.	1.5	40
51	Cold spray deposition of an icosahedral-phase-strengthened aluminum alloy coating. Surface and Coatings Technology, 2017, 324, 57-63.	2.2	40
52	Nucleation of the lamellar decomposition in a Ti–44Al–4Nb–4Zr alloy. Acta Materialia, 2004, 52, 191-197.	3.8	39
53	Carbon aerogel supported nickel nanoparticles and nanorods using supercritical deposition. Journal of Supercritical Fluids, 2012, 66, 265-273.	1.6	39
54	Thickness dependence of electronic phase transitions in epitaxial V2O3 films on (0001) LiTaO3. Applied Physics Letters, 2008, 93, .	1.5	38

#	Article	IF	CITATIONS
55	Characterization of the Fe-Doped Mixed-Valent Tunnel Structure Manganese Oxide KOMS-2. Journal of Physical Chemistry C, 2011, 115, 21610-21619.	1.5	38
56	Characterization of the microstructure and phase equilibria calculations for the powder metallurgy superalloy IN100. Journal of Materials Research, 2003, 18, 2653-2663.	1.2	37
57	Techniques for microstructural characterization of powder-processed nickel-based superalloys. Materials Science & Engineering A: Structural Materials: Properties, Microstructure and Processing, 2003, 360, 390-395.	2.6	36
58	Control of average particle size of carbon aerogel supported platinum nanoparticles by supercritical deposition. Microporous and Mesoporous Materials, 2017, 245, 94-103.	2.2	36
59	Focused Ion Beam Preparation of Specimens for Micro-Electro-Mechanical System-based Transmission Electron Microscopy Heating Experiments. Microscopy and Microanalysis, 2017, 23, 708-716.	0.2	36
60	Precipitate orientation relationships and interfacial structures in duplex stainless steel Zeron-100. Philosophical Magazine, 2003, 83, 1867-1887.	0.7	35
61	Threading dislocation generation in epitaxial (Ba,Sr) TiO3 films grown on (001) LaAlO3 by pulsed laser deposition. Applied Physics Letters, 2004, 84, 1742-1744.	1.5	35
62	Hydrogen-assisted stable crack growth in iron-3 wt% silicon steel. Acta Materialia, 1996, 44, 3125-3140.	3.8	34
63	Defect microstructures in epitaxial PbZr0.2Ti0.8O3 films grown on (001) SrTiO3 by pulsed laser deposition. Journal of Materials Science, 2006, 41, 697-707.	1.7	34
64	Modification of carbon aerogel supports for PEMFC catalysts. International Journal of Hydrogen Energy, 2009, 34, 8992-8997.	3.8	34
65	Topographical development and misfit relief in laser-ablated heteroepitaxial YBa2Cu3O7â^îŕ thin films. Journal of Crystal Growth, 1997, 172, 145-155.	0.7	33
66	A high-resolution electron microscopy study of steps on lamellar γ-α <sub>2</sub> interfaces in a low-misfit TiAl-based alloy. Philosophical Magazine A: Physics of Condensed Matter, Structure, Defects and Mechanical Properties, 1999, 79, 2553-2575.	0.8	33
67	Thermodynamic and electrostatic analysis of threading dislocations in epitaxial ferroelectric films. Applied Physics Letters, 2006, 88, 102906.	1.5	32
68	Unraveling the Mesoscale Evolution of Microstructure during Supersonic Impact of Aluminum Powder Particles. Scientific Reports, 2018, 8, 10075.	1.6	31
69	Deformation mechanisms in intermetallic compounds based on Nb3Al. Materials Science & Engineering A: Structural Materials: Properties, Microstructure and Processing, 1993, 170, 1-10.	2.6	29
70	Nanostructured arrays of semiconducting octahedral molecular sieves by pulsed-laser deposition. Nature Materials, 2010, 9, 54-59.	13.3	29
71	A Foaming Esterification Sol–Gel Route for the Synthesis of Magnesia–Yttria Nanocomposites. Journal of the American Ceramic Society, 2011, 94, 367-371.	1.9	29
72	Modified Mesoporous Silica for Efficient Siloxane Capture. Langmuir, 2016, 32, 2369-2377.	1.6	29

#	Article	IF	CITATIONS
73	Microstructure and Micromechanical Response in Gas-Atomized Al 6061 Alloy Powder and Cold-Sprayed Splats. Journal of Thermal Spray Technology, 2018, 27, 1563-1578.	1.6	29
74	Deformation behaviour of the C15 Laves phase Cr2Nb. Materials Science & Engineering A: Structural Materials: Properties, Microstructure and Processing, 1997, 233, 44-49.	2.6	28
75	Incorporation of fluorine ions into hydroxyapatite by a pH cycling method. Journal of Materials Science: Materials in Medicine, 2005, 16, 447-453.	1.7	28
76	Constitutive modeling of high temperature flow behavior in a Ti-45Al-8Nb-2Cr-2Mn-0.2Y alloy. Scientific Reports, 2018, 8, 5453.	1.6	28
77	Effects of Precursor Chemistry on the Structural Characteristics of Y <sub>2</sub> O <sub>3</sub> –MgO Nanocomposites Synthesized by a Combined Sol–Gel/Thermal Decomposition Route. Journal of the American Ceramic Society, 2011, 94, 372-381.	1.9	27
78	Influence of electric current on microstructure evolution in Ti/Al and Ti/TiAl3 during spark plasma sintering. Journal of Alloys and Compounds, 2015, 648, 1097-1103.	2.8	27
79	Comparison of virgin Ti-6Al-4V powders for additive manufacturing. Additive Manufacturing, 2018, 21, 544-555.	1.7	27
80	The effect of finely dispersed particles on primary recrystallisation textures in AlMnSi alloys. Materials Science & Engineering A: Structural Materials: Properties, Microstructure and Processing, 1997, 225, 9-21.	2.6	26
81	The stoichiometry of metal assisted etching (MAE) of Si in V2O5+HF and HOOH+HF solutions. Electrochimica Acta, 2015, 158, 219-228.	2.6	26
82	Mesoporous carbon aerogel supported PtCu bimetallic nanoparticles via supercritical deposition and their dealloying and electrocatalytic behaviour. Catalysis Today, 2018, 310, 166-175.	2.2	26
83	Geometry and interface structure of island nuclei for GaSb buffer layers grown on (001) GaAs by metalorganic vapour phase epitaxy. Journal of Crystal Growth, 1993, 133, 168-174.	0.7	25
84	Hydrodesulfurization of model diesel using Pt/Al2O3 catalysts prepared by supercritical deposition. Catalysis Today, 2005, 99, 365-373.	2.2	25
85	Aerogel–copper nanocomposites prepared using the adsorption of a polyfluorinated complex from supercritical CO2. Journal of Nanoparticle Research, 2012, 14, 1.	0.8	25
86	Structure and mechanical properties in a powder-processed icosahedral-phase-strengthened aluminum alloy. Scripta Materialia, 2016, 123, 51-54.	2.6	25
87	Regenerative Electroless Etching of Silicon. Angewandte Chemie - International Edition, 2017, 56, 624-627.	7.2	25
88	High-pressure torsion-induced phase transformations and grain refinement in Al/Ti composites. Journal of Materials Science, 2017, 52, 12170-12184.	1.7	25
89	The origins of growth spirals on laser-ablated YBa2Cu3O7-δ thin films. Philosophical Magazine Letters, 1994, 70, 47-53.	0.5	24
90	Development of quasicrystal morphology in gas-atomized icosahedral-phase-strengthened aluminum alloy powders. Materials and Design, 2019, 182, 108094.	3.3	24

#	Article	IF	CITATIONS
91	On epitaxial misorientations. Philosophical Magazine A: Physics of Condensed Matter, Structure, Defects and Mechanical Properties, 1991, 63, 667-694.	0.8	23
92	Phase stability in a powder-processed Al–Mn–Ce alloy. Journal of Materials Science, 2014, 49, 3742-3754.	1.7	23
93	Electrostatically driven dielectric anomaly in mesoscopic ferroelectric–paraelectric bilayers. Acta Materialia, 2016, 105, 68-74.	3.8	23
94	Concerning the dissociation of grown-in dislocations in melt spun ribbons of the intermetallic compound Nb <sub>3</sub> Al. Philosophical Magazine Letters, 1991, 64, 59-65.	0.5	22
95	Focused ion beam sectioning studies of biomimetic hydroxyapatite coatings on Ti-6Al-4V substrates. Surface and Coatings Technology, 2017, 313, 255-262.	2.2	22
96	Eutectic microstructures in dilute Al-Ce and Al-Co alloys. Materials Characterization, 2019, 154, 269-276.	1.9	22
97	Observation of a metastable B2 phase in rapidly solidified ribbons of Nbî—,Al alloys. Scripta Metallurgica Et Materialia, 1993, 29, 1271-1274.	1.0	21
98	The Influence of Oxide Layers on the Initiation of Carbon Deposition on Stainless Steel. Oxidation of Metals, 2001, 56, 231-250.	1.0	21
99	VULCAN-SUPPORTED Pt ELECTROCATALYSTS FOR PEMFCs PREPARED USING SUPERCRITICAL CARBON DIOXIDE DEPOSITION. Chemical Engineering Communications, 2008, 196, 194-203.	1.5	21
100	Phase Homogeneity in <scp><scp>Y</scp><sub>2</sub><scp>O</scp><sub>3</sub>–<scp>MgO</scp></scp> Nanocomposites Synthesized by Thermal Decomposition of Nitrate Precursors with Ammonium Acetate Additions. Journal of the American Ceramic Society, 2011, 94, 4207-4217.	1.9	21
101	A study of the Pd/highly oriented pyrolytic graphite electrodeposition system by in situ electrochemical scanning tunnelling microscopy. Journal of Electroanalytical Chemistry, 1995, 395, 117-126.	1.9	20
102	Effects of Zn coating on the microstructure and magnetic properties of Nd–Fe–B magnets. Journal of Alloys and Compounds, 2003, 351, 299-303.	2.8	20
103	STRONG DEGRADATION OF PHYSICAL PROPERTIES AND FORMATION OF A DEAD LAYER IN FERROELECTRIC FILMS DUE TO INTERFACIAL DISLOCATIONS. Integrated Ferroelectrics, 2005, 71, 67-80.	0.3	20
104	A Sucroseâ€Mediated Sol–Gel Technique for the Synthesis of <scp><scp>MgO</scp></scp> – <scp>Y</scp> <sub>2</sub> <scp><scp>O</scp></scp> <sub>3Nanocomposites. Journal of the American Ceramic Society, 2013, 96, 346-350.</sub>	ubø	20
105	Microstructure and preparation of an ultra-fine-grained W-Al 2 O 3 composite via hydrothermal synthesis and spark plasma sintering. International Journal of Refractory Metals and Hard Materials, 2018, 72, 149-156.	1.7	20
106	Stability and work function of <mml:math <br="" xmlns:mml="http://www.w3.org/1998/Math/MathML">display="inline"&gt;<mml:mrow><mml:msub><mml:mrow><mml:mtext>TiC</mml:mtext></mml:mrow><mml:mi>x&lt; surfaces: Density functional theory calculations. Physical Review B, 2009, 80, .</mml:mi></mml:msub></mml:mrow></mml:math>	/maml:mi>	< <b>រ្វា</b> ml:msub
107	Microstructural effects of the reduction step in reactive consolidation of manganese cobaltite coatings on Crofer 22 APU. Materials at High Temperatures, 2015, 32, 142-147.	0.5	19
108	Salt fog corrosion behavior in a powder-processed icosahedral-phase-strengthened aluminum alloy. Corrosion Science, 2017, 121, 133-138.	3.0	19

#	Article	IF	CITATIONS
109	Temperature calibration of TEM specimen heating holders by isothermal sublimation of silver nanocubes. Ultramicroscopy, 2019, 196, 142-153.	0.8	19
110	Highly Active Carbon Supported PtCu Electrocatalysts for PEMFCs by <i>in situ</i> Supercritical Deposition Coupled with Electrochemical Dealloying. Fuel Cells, 2020, 20, 285-299.	1.5	19
111	On the influence of stoichiometry and purity on the deformation mechanisms in the intermetallic compound TiAl. Scripta Metallurgica Et Materialia, 1990, 24, 1105-1108.	1.0	18
112	Band-Edge Photoluminescence Recovery from Zinc-Blende CdSe Nanocrystals Synthesized at Room Temperature. Advanced Functional Materials, 2006, 16, 345-350.	7.8	18
113	Electrochemical performance of fuel cell catalysts prepared by supercritical deposition: Effect of different precursor conversion routes. Journal of Supercritical Fluids, 2015, 97, 154-164.	1.6	18
114	The influence of substrate surface preparation on the microstructure of CdTe grown on (001) GaAs by metalorganic chemical vapour deposition. Journal of Crystal Growth, 1994, 135, 409-422.	0.7	17
115	Stacking-fault energy in the C15 Laves phase Cr2Nb. Philosophical Magazine Letters, 1996, 74, 129-136.	0.5	17
116	On the self-pinning character of synchro-Shockley dislocations in a Laves phase during strain rate cyclical compressions. Scripta Materialia, 2008, 59, 788-791.	2.6	17
117	Phase Homogeneity in MgO–ZrO <sub>2</sub> Nanocomposites Synthesized by a Combined Sol–Gel/Thermal Decomposition Route. Journal of the American Ceramic Society, 2010, 93, 3102-3109.	1.9	17
118	Shock-induced deformation twinning and softening in magnesium single crystals. Materials and Design, 2020, 194, 108884.	3.3	17
119	Thermally activated structural transformations in manganese oxide nanoparticles under air and argon atmospheres. Journal of Materials Science, 2020, 55, 7247-7258.	1.7	17
120	A transmission electron microscope study of microstructural development in magnetron-sputtered MoSi2 thin films. Intermetallics, 2002, 10, 829-839.	1.8	16
121	Heteroepitaxial Growth of Nanoscale Oxide Shell/Fiber Superstructures by Mild Hydrothermal Processes. Small, 2010, 6, 988-992.	5.2	16
122	Transformation of La0.65Sr0.35MnO3 in electrochemical water oxidation. International Journal of Hydrogen Energy, 2017, 42, 8560-8568.	3.8	16
123	Crystallographically Determined Etching and Its Relevance to the Metal-Assisted Catalytic Etching (MACE) of Silicon Powders. Frontiers in Chemistry, 2019, 6, 651.	1.8	16
124	Studies of thermally activated processes in gas-atomized Al alloy powders: in situ STEM heating experiments on FIB-cut cross sections. Journal of Materials Science, 2019, 54, 9921-9932.	1.7	16
125	Multifunctional transition metal doped titanium dioxide reduced graphene oxide composites as highly efficient adsorbents and photocatalysts. Microporous and Mesoporous Materials, 2020, 307, 110521.	2.2	16
126	Dislocation Motion in λ Tial Studied by in situ Straining Experiments in the Hvem. Materials Research Society Symposia Proceedings, 1994, 364, 47.	0.1	15

#	Article	IF	CITATIONS
127	Formation and microstructural development of TiSi2 in (111)Si by Ti ion implantation and annealing at 950 °C. Journal of Materials Research, 1995, 10, 891-899.	1.2	15
128	Microstructures and deformation behaviour in Nb/10–25at.% Al/20–40at.%V alloys. Acta Materialia, 1997, 45, 4923-4938.	3.8	15
129	Microstructure and mechanical behaviour of Nb–Al–V alloys with 10–25 at.% Al and 20–40 at.% V—I: microstructural observations. Intermetallics, 2002, 10, 1-12.	1.8	15
130	The effect of Mn1.5Co1.5O4 coatings on the development of near surface microstructure for Haynes 230 oxidized at 800°C in air. Surface and Coatings Technology, 2014, 242, 109-117.	2.2	15
131	A Comparative Study of the Nanocrystalline Material Produced by Sliding Wear and Inert Gas Condensation. Materials Research Society Symposia Proceedings, 1990, 206, 593.	0.1	14
132	The Stability of B2 Compounds in Ti-Modified Nb-Al Alloys. Materials Research Society Symposia Proceedings, 1992, 288, 243.	0.1	14
133	Effect of heat-treatment on the microstructure and hardness of a devitrified Al–3.0Y–3.0Gd–5.0Ni–1.0Fe–1.0Co alloy. Scripta Materialia, 2004, 51, 485-489.	2.6	14
134	Magnetic and tunable dielectric properties of DyCrO3 thin films. Journal of Materials Science, 2019, 54, 8984-8994.	1.7	14
135	Low-Load Metal-Assisted Catalytic Etching Produces Scalable Porosity in Si Powders. ACS Applied Materials & Interfaces, 2020, 12, 48969-48981.	4.0	14
136	Microstructure/mechanical behavior relationships in upset-forged powder-processed Al alloys containing icosahedral quasicrystalline dispersoids. Materials Science & Engineering A: Structural Materials: Properties, Microstructure and Processing, 2020, 788, 139487.	2.6	14
137	Surface states of gas-atomized Al 6061 powders – Effects of heat treatment. Applied Surface Science, 2020, 534, 147643.	3.1	14
138	Effect of laser scan length on the microstructure of additively manufactured 17-4PH stainless steel thin-walled parts. Additive Manufacturing, 2020, 35, 101302.	1.7	14
139	The effect of substrate-off-cut on the properties of epitaxial thin films of YBa2Cu3O7â^Î^ grown by pulsed laser deposition. Applied Surface Science, 1998, 127-129, 525-530.	3.1	13
140	Nanoscale carbide precipitation in the recast layer of a percussion laser-drilled superalloy. Scripta Materialia, 2009, 61, 943-946.	2.6	13
141	Base metal alloys with self-healing native conductive oxides for electrical contact materials. Applied Physics Letters, 2010, 97, .	1.5	13
142	Hexagonal crystallography and interphase boundary dislocations. Scripta Metallurgica, 1987, 21, 971-974.	1.2	12
143	In situ electrochemical scanning probe microscopy corrosion studies on duplex stainless steel in aqueous NaCl solutions. Corrosion Engineering Science and Technology, 1996, 31, 139-146.	0.3	12
144	Microstructure and mechanical behaviour of Nb–Al–V alloys with 10–25 at.% Al and 20–40 at.% V—II: mechanical behaviour and deformation mechanisms. Intermetallics, 2002, 10, 13-21.	1.8	12

#	Article	IF	CITATIONS
145	Polymorphism in the Laves-phase precipitates of a quinternary Nb–Mo–Cr–Al–Si alloy. Scripta Materialia, 2009, 60, 72-75.	2.6	12
146	A Comparison of Ga FIB and Xe-Plasma FIB of Complex Al Alloys. Microscopy and Microanalysis, 2017, 23, 288-289.	0.2	12
147	Interfacial Structure in Heteroepitaxial Silicon on Sapphire. Journal of the American Ceramic Society, 1990, 73, 1136-1143.	1.9	11
148	Development of anisotropic microtwin distributions in GaAs grown on 4°â€off (001) Si by molecular beam epitaxy. Applied Physics Letters, 1994, 65, 1903-1905.	1.5	11
149	Annealing twins in dilute Al[sbnd]Mn[sbnd]Si alloys. Philosophical Magazine Letters, 1995, 72, 193-198.	0.5	11
150	The interaction between extended dislocations and antiphase domain boundaries— I: superpartial separation and the yield stress. Intermetallics, 2001, 9, 499-506.	1.8	11
151	Microstructural characteristics of the eutectoid mixture Zr2Cu and Zr7Cu10. Journal of Materials Science Letters, 2001, 20, 543-545.	0.5	11
152	Morphology and interfacial structure of gamma precipitates in the beta phase of a Ti-Al-Nb-Zr alloy. Journal of Materials Science, 2006, 41, 611-619.	1.7	11
153	Microstructural stability and phase transformations in electrodeposited cobalt-phosphorus coatings. Journal of Alloys and Compounds, 2017, 719, 142-150.	2.8	11
154	Mechanical properties of supersonic-impacted Al6061 powder particles. Scripta Materialia, 2019, 171, 52-56.	2.6	11
155	Controlling the Nature of Etched Si Nanostructures: High- versus Low-Load Metal-Assisted Catalytic Etching (MACE) of Si Powders. ACS Applied Materials & Interfaces, 2020, 12, 4787-4796.	4.0	11
156	Precipitation phenomena in a powder-processed quasicrystal-reinforced Al-Cr-Mn-Co-Zr alloy. Materials Characterization, 2021, 178, 111239.	1.9	11
157	The Effect of Rapid Thermal Annealing on the Dislocation Structure of Silicon on Sapphire. Materials Research Society Symposia Proceedings, 1988, 138, 373.	0.1	10
158	High-resolution electron microscopy of steps on misfitting lamellar Î <sup>3</sup> -α2interfaces in a Ti-44at.% Al-8at.% Nb alloy. Philosophical Magazine Letters, 2000, 80, 1-10.	0.5	10
159	Zn diffusion induced precipitation along grain boundaries in Zn-coated NdFeB magnets. Journal of Magnetism and Magnetic Materials, 2003, 261, 13-20.	1.0	10
160	Electrical and tribological properties of a Ni–18%Ru alloy for contact applications. Journal of Materials Science, 2011, 46, 6563-6570.	1.7	10
161	Microstructure effects in braze joints formed between Ag/W electrical contacts and Sn-coated Cu using Cu–Ag–P filler metal. Journal of Materials Science, 2015, 50, 324-333.	1.7	10
162	Solidification microstructures in Ag3Sn–Cu3Sn pseudo-binary alloys. Journal of Materials Science, 2016, 51, 6474-6487.	1.7	10

#	Article	IF	CITATIONS
163	Preparation of Pt/Al2O3 and PtPd/Al2O3 catalysts by supercritical deposition and their performance for oxidation of nitric oxide and propene. Catalysis Today, 2022, 388-389, 70-78.	2.2	10
164	Defects in Large-Misfit Heteroepitaxy. Materials Research Society Symposia Proceedings, 1988, 116, 267.	0.1	9
165	Reassessment of the constrained coincident-site-lattice model for reference structures in vicinal high-angle grain boundaries. Philosophical Magazine Letters, 1997, 76, 25-32.	O.5	9
166	Synthesis of Novel Electrode Materials Using Supercritical Fluids. ECS Transactions, 2009, 19, 9-21.	0.3	9
167	Characterization of microstructural effects in a percussion laser-drilled powder metallurgy Ni-based superalloy. Journal of Materials Science, 2009, 44, 680-684.	1.7	9
168	Supercritical Deposition Coupled with Ammonia Treatment: A New Route to Coâ€Promoted Nâ€Doped Carbon Aerogels with High Oxygen Reduction Reaction Activity. Energy Technology, 2019, 7, 1900450.	1.8	9
169	Corrosion phenomena in a powder-processed Al alloy containing icosahedral quasicrystalline dispersoids. Corrosion Science, 2020, 177, 108970.	3.0	9
170	Deformation Mechanisms and Mechanical Properties of B2 Compounds in Ti-Modified Nb-Al Alloys. Materials Research Society Symposia Proceedings, 1992, 288, 573.	0.1	8
171	Self-assembly of size-selected colloidal metal clusters: Crystalline descriptions of non-close-packed arrangements. Philosophical Magazine Letters, 1999, 79, 569-574.	0.5	8
172	Microstructure of laser-ablated superconducting La <sub>2</sub> CuO <sub>4</sub> F <sub><i>x</i></sub> thin films on SrTiO <sub>3</sub> . Journal of Materials Research, 2001, 16, 3309-3316.	1.2	8
173	Oxygen-stabilised partial amorphisation in a Zr50Cu50 alloy. Journal of Materials Science, 2002, 37, 745-751.	1.7	8
174	Phase formation during the devitrification of Al-rich melt-spun Al?8.5Ni?5.0Y?3.0(Co,Fe) alloys. Scripta Materialia, 2005, 52, 699-704.	2.6	8
175	A hybrid replication technique for the analysis of precipitate-boundary interactions in Ni-based superalloys. Journal of Materials Science, 2005, 40, 3403-3407.	1.7	8
176	The structure of ternary compounds in a devitrified Al-rich Al–Ni–Gd alloy. Intermetallics, 2005, 13, 741-748.	1.8	8
177	The microstructural evolution of NbAIV ternary alloys. Intermetallics, 2005, 13, 1157-1165.	1.8	8
178	Cation ordering in epitaxial lead zirconate titanate films. Applied Physics Letters, 2008, 93, 262903.	1.5	8
179	Synthesis of Ru/PDMS nano-composites via supercritial deposition. Materials Chemistry and Physics, 2016, 180, 1-4.	2.0	8
180	Superelastic and micaceous deformation in the intermetallic compound CaFe2As2. Scripta Materialia, 2017, 141, 10-14.	2.6	8

#	Article	IF	CITATIONS
181	Microstructural stability, defect structures and deformation mechanisms in a Ag3Sn/Cu3Sn alloy. Journal of Materials Science, 2017, 52, 2944-2956.	1.7	8
182	Hierarchical Nanostructuring of Porous Silicon with Electrochemical and Regenerative Electroless Etching. ACS Nano, 2019, 13, 13056-13064.	7.3	8
183	Analysis of the reference structure adopted by a mixed tilt-twist vicinal high-angle grain boundary in titanium. Philosophical Magazine A: Physics of Condensed Matter, Structure, Defects and Mechanical Properties, 1997, 76, 871-888.	0.8	7
184	The Effect of Etchant Composition on Film Structure during Laser-Assisted Porous Si Growth. Physica Status Solidi A, 2000, 182, 87-91.	1.7	7
185	High-resolution transmission electron microscopy studies of planar defects in the magnetic superconductor RuSr2EuCu2O8. Applied Physics Letters, 2004, 85, 3217-3219.	1.5	7
186	Effects of microstructure on native oxide scale development and electrical characteristics of eutectic Cu–Cu6La alloys. Acta Materialia, 2012, 60, 851-859.	3.8	7
187	Effect of upset forging on microstructure and tensile properties in a devitrified Al–Ni–Co–Y Alloy. Journal of Materials Science, 2013, 48, 3841-3851.	1.7	7
188	Microstructural evolution in manganese cobaltite films grown on Crofer 22 APU substrates by pulsed laser deposition. Surface and Coatings Technology, 2016, 286, 206-214.	2.2	7
189	Ion-damage-free planarization or shallow angle sectioning of solar cells for mapping grain orientation and nanoscale photovoltaic properties. Nanotechnology, 2017, 28, 185705.	1.3	7
190	An Electron Microscopy Study of the Microstructure and Microarchitecture of the <i>Strombus Gigas</i> Shell. Materials Research Society Symposia Proceedings, 1989, 174, 117.	0.1	6
191	On the shape of edge-dislocation loops in $\hat{I}^2$ NiAl. Philosophical Magazine Letters, 1990, 62, 317-322.	0.5	6
192	The role of the initial nucleation stage in microstructural development for CdTe grown on heat-cleaned 2°-off (001)GaAs by metalorganic chemical vapour deposition. Journal of Crystal Growth, 1995, 154, 251-261.	0.7	6
193	The application of pettifor structure maps to ternary additions in Nb3Al-based alloys. Scripta Materialia, 1996, 34, 227-234.	2.6	6
194	Structural imaging of mechanically alloyed remanence-enhanced Sm2Fe17N3/α-Fe. Journal of Magnetism and Magnetic Materials, 1996, 157-158, 79-80.	1.0	6
195	Extraction replication studies of near-surface microstructures in laser-drilled samples of the powder metallurgy Ni-based superalloy IN100. Materials Characterization, 2010, 61, 929-936.	1.9	6
196	Surface Degradation of Ag/W Circuit Breaker Contacts During Standardized UL Testing. Journal of Materials Engineering and Performance, 2015, 24, 3251-3262.	1.2	6
197	Strong, ductile, and thermally stable Cu-based metal-intermetallic nanostructured composites. Scientific Reports, 2017, 7, 40409.	1.6	6
198	Characterization of IrOx sputtering for IrO2 and IrO2/Pt bottom-electrode piezoelectric micro-electro-mechanical systems applications. Thin Solid Films, 2017, 638, 127-137.	0.8	6

#	Article	IF	CITATIONS
199	Defect structures in solution-grown single crystals of the intermetallic compound Ag3Sn. Journal of Materials Science, 2018, 53, 5317-5328.	1.7	6
200	Insights into the plasticity of Ag3Sn from density functional theory. International Journal of Plasticity, 2018, 110, 57-73.	4.1	6
201	A Promising Catalyst for the Dehydrogenation of Perhydro-Dibenzyltoluene: Pt/Al2O3 Prepared by Supercritical CO2 Deposition. Catalysts, 2022, 12, 489.	1.6	6
202	Dislocations and Slip Systems in V3Si. Materials Research Society Symposia Proceedings, 1992, 288, 477.	0.1	5
203	Misfit dislocations in laser-ablated heteroepitaxial YBa2Cu3O7-delta on MgO(001). Philosophical Magazine Letters, 1996, 74, 267-272.	0.5	5
204	On the Effect of Antiphase Domain Boundaries on ALCHEMI. Physica Status Solidi (B): Basic Research, 1999, 214, 237-243.	0.7	5
205	Identifying the character of intrinsic stacking faults in the A15 compound Nb3Al. Philosophical Magazine Letters, 2000, 80, 519-524.	0.5	5
206	The interaction between extended dislocations and antiphase domain boundaries— II: uncoupled superpartial dislocations and planar slip. Intermetallics, 2001, 9, 507-514.	1.8	5
207	Observation of tension/compression asymmetry in an Nb–Al–V alloy. Materials Science & Engineering A: Structural Materials: Properties, Microstructure and Processing, 2004, 387-389, 476-480.	2.6	5
208	Characterization of Metallurgical Effects in Laser-Drilling of Superalloys. Microscopy and Microanalysis, 2008, 14, 558-559.	0.2	5
209	Atomic site occupancies and mechanical response of the eutectic C14 and A15 phases in a quinternary Nb–Mo–Cr–Al–Si alloy. Scripta Materialia, 2009, 60, 309-312.	2.6	5
210	Microstructural Characteristics of Y2O3-MgO Composite Coatings Deposited by Suspension Plasma Spray. Journal of Thermal Spray Technology, 2012, 21, 1309-1321.	1.6	5
211	Effect of heat-treatment on phase stability and grain coarsening in a powder-processed Al–Ni–Co–Zr–Y alloy. Journal of Materials Science, 2014, 49, 5866-5877.	1.7	5
212	Switchable and tunable film bulk acoustic resonator fabricated using barium strontium titanate active layer and Ta2O5/SiO2 acoustic reflector. Applied Physics Letters, 2016, 109, .	1.5	5
213	Metalorganic solution deposition of lead zirconate titanate films onto an additively manufactured Ni-based superalloy. Acta Materialia, 2017, 122, 352-358.	3.8	5
214	Hydrogen annealing effects on local structures and oxidation states of atomic layer deposited SnOx. Journal of Vacuum Science and Technology A: Vacuum, Surfaces and Films, 2018, 36, .	0.9	5
215	Threading dislocations in chemical-vapour-deposited β-SiC on (001)Si. Philosophical Magazine Letters, 1990, 62, 239-246.	0.5	4
216	On the extension of substrate dislocations into heteroepitaxial deposits. Philosophical Magazine Letters, 1990, 62, 139-141.	0.5	4

#	Article	IF	CITATIONS
217	Use of ferrofluids to obtain magnetic domain images in afm. Microscopy Research and Technique, 1992, 23, 98-99.	1.2	4
218	Analysis of the dislocation network at a low-angle near-twist boundary in zinc. Scripta Metallurgica Et Materialia, 1993, 29, 811-816.	1.0	4
219	On the origins of â€~forbidden' 100-type spots in electron diffraction patterns from the A15 compounds Nb <sub>3</sub> Al, Cr <sub>3</sub> Si and V <sub>3</sub> Si. Philosophical Magazine Letters, 1994, 69, 23-30.	0.5	4
220	Microstructures and properties of laser-ablated epitaxial Y-Ba-Cu-O thin films for electronic device applications. IEEE Transactions on Applied Superconductivity, 1995, 5, 1214-1217.	1.1	4
221	TEM Studies Of Devitrification Products in Al-Gd-Ni-(Fe) Alloys Materials Research Society Symposia Proceedings, 2003, 806, 256.	0.1	4
222	Î <sup>3</sup> ' Precipitation Kinetics in P/M IN100. Materials Science Forum, 2003, 426-432, 767-772.	0.3	4
223	Grain Boundary Curvature in a Model Ni-Based Superalloy. Metallurgical and Materials Transactions A: Physical Metallurgy and Materials Science, 2007, 38, 1-6.	1.1	4
224	Microstructure and phase stability in a Nb–Mo–Cr–Al–Si alloy. Journal of Materials Science, 2008, 43, 7013-7025.	1.7	4
225	Substrate Control of Anisotropic Resistivity in Heteroepitaxial Nanostructured Arrays of Cryptomelane Manganese Oxide on Strontium Titanate. Small, 2014, 10, 66-72.	5.2	4
226	ALCHEMI studies of site occupancies in Cr-, Ni-, and Fe-substituted manganese cobaltite spinels. Journal of Materials Science, 2016, 51, 158-170.	1.7	4
227	Regenerative Electroless Etching of Silicon. Angewandte Chemie, 2017, 129, 639-642.	1.6	4
228	Effect of IrO2/Pt, IrO2, and Pt bottom electrodes on the structure and electrical properties of PZT based piezoelectric microelectromechanical system devices. Journal of Materials Science: Materials in Electronics, 2018, 29, 11367-11377.	1.1	4
229	A Nanoindentation Study of the Plastic Deformation and Fracture Mechanisms in Single-Crystalline CaFe2As2. Jom, 2018, 70, 1074-1080.	0.9	4
230	Surfactant selection as a strategy for tailoring the structure and properties of UCT manganese oxides. Materials and Design, 2019, 180, 107902.	3.3	4
231	Fabrication of a multi-phase porous high-temperature Mo–Si–B alloy by <i>in situ</i> reaction synthesis. Powder Metallurgy, 2019, 62, 258-266.	0.9	4
232	Uniaxial compression of [001]-oriented CaFe2As2 single crystals:the effects of microstructure and temperature on superelasticity Part I: Experimental observations. Acta Materialia, 2021, 203, 116464.	3.8	4
233	Thermal stability of quasicrystals in an icosahedral-phase-strengthened aluminum alloy. Materials Characterization, 2021, 181, 111490.	1.9	4
234	Compatibility of Potential Reinforcing Ceramics with Ni and Fe Aluminides. Materials Research Society Symposia Proceedings, 1990, 194, 379.	0.1	3

#	Article	IF	CITATIONS
235	The Use of Electrochemical Scanning Tunneling Microscopy to Study the Initial Stages of Electrodeposition <i>in situ</i> ; Overpotential Deposition of Pb and Pt on HOPG. Transactions of the Institute of Metal Finishing, 1992, 70, 171-176.	0.6	3
236	A Modified Approach to the Modelling of Grain Boundary Structure in Materials with an Hexagonal Crystal Structure. Materials Research Society Symposia Proceedings, 1993, 319, 251.	0.1	3
237	Microstructures, Defects and Deformation Mechanisms in Vanadium Modified Nb3Al. Materials Research Society Symposia Proceedings, 1993, 322, 453.	0.1	3
238	Precipitation and migration of point defects in MOCVD Cd Hg1 â^' Te. Journal of Crystal Growth, 1996, 159, 1096-1099.	0.7	3
239	The effects of Al substitution on the microstructure and properties of laser-ablated epitaxial YBa2Cu3O7â^Î films on (001) MgO. Physica C: Superconductivity and Its Applications, 1997, 274, 117-124.	0.6	3
240	The Character of Steps on Gamma/Alpha-2 Interfaces in Lamellar TiAl-Based Alloys. Materials Science Forum, 1999, 294-296, 239-242.	0.3	3
241	On the orientation relationships between A15 precipitates and the Nb-rich matrix in Nb-Al(-X) alloys. Philosophical Magazine Letters, 1999, 79, 93-98.	0.5	3
242	Orientational and translational ordering of sub-monolayer films of passivated multiply-twinned gold clusters. Journal Physics D: Applied Physics, 2000, 33, L23-L26.	1.3	3
243	Defect formation in Nd2Fe14B grains caused by Zn diffusion. Philosophical Magazine Letters, 2001, 81, 233-241.	0.5	3
244	Phase Transformations in Equiatomic ZrCu Alloy. Journal of Metastable and Nanocrystalline Materials, 2001, 10, 223-228.	0.1	3
245	Phase Transformations in Equiatomic ZrCu Alloy. Materials Science Forum, 2001, 360-362, 223-228.	0.3	3
246	Adoption of near-coincident-site lattice orientations by contacting monolayer rafts of metallic nanoparticles with different superlattice periodicities. Philosophical Magazine Letters, 2002, 82, 21-26.	0.5	3
247	Devitrification Mechanisms in Al-Y-Ni Glasses. Materials Research Society Symposia Proceedings, 2003, 806, 108.	0.1	3
248	Interfacial Defects and Lamellar Decomposition in Titanium Aluminides. Journal of Materials Science, 2004, 12, 293-302.	1.2	3
249	Accommodation of angular incompatibilities between interfacial facets during precipitate growth. Metallurgical and Materials Transactions A: Physical Metallurgy and Materials Science, 2006, 37, 901-909.	1.1	3
250	The influence of pulse parameters on the laser drilling of hastelloy X. , 2007, , .		3
251	FIB Milling strategies for TEM Sample Preparation of Spheroidal Powder Particles. Microscopy and Microanalysis, 2018, 24, 826-827.	0.2	3
252	Hierarchical Porous Silicon and Porous Silicon Nanowires Produced with Regenerative Electroless Etching (ReEtching) and Metal Assisted Catalytic Etching (MACE). ECS Transactions, 2018, 86, 65-70.	0.3	3

#	Article	IF	CITATIONS
253	Effect of transition metal alloying elements on the deformation of Ti-44Al-8Nb-0.2B-0.2Y alloys. Scientific Reports, 2018, 8, 14242.	1.6	3
254	Aerobic Selfâ€Esterification of Alcohols Assisted by Mesoporous Manganese and Cobalt Oxide. ChemCatChem, 2019, 11, 3413-3422.	1.8	3
255	Heterogeneous Distribution of Mechanical Properties of Single-Particle Cold Spray Impacts. Journal of Thermal Spray Technology, 2022, 31, 498-507.	1.6	3
256	Metastable Phases and Defect Microstructures in Melt-Spun Ribbons of Nb3Al. Materials Research Society Symposia Proceedings, 1990, 209, 89.	0.1	2
257	Planar Growth Faults in Nb3Al. Materials Research Society Symposia Proceedings, 1992, 288, 263.	0.1	2
258	Microscopic studies of YBCO single crystals. Journal of Crystal Growth, 1993, 128, 762-766.	0.7	2
259	Structure of a 12.29° near-tilt grain boundary in titanium. Philosophical Magazine Letters, 1996, 73, 217-224.	0.5	2
260	Crystallization of Glassy Powder from Aluminum-Rare Earth- Transition Metal Alloys. Materials Research Society Symposia Proceedings, 2002, 754, 1.	0.1	2
261	Measurement of epitaxial misorientations and related effects in thin films of YBa2Cu3O7-δ grown on nominally (001)MgO substrates by pulsed laser deposition. Thin Solid Films, 2003, 423, 33-40.	0.8	2
262	Extraction Replication of Carbides and Borides in the Ni-base Superalloy IN100. Microscopy and Microanalysis, 2004, 10, 692-693.	0.2	2
263	HREM of Carbide and Silicide Precipitation in a TiAl-Based Alloy During Aging. Microscopy and Microanalysis, 2004, 10, 702-703.	0.2	2
264	Characterization of the Surface Layer of Ag/W Electrical Contacts. Microscopy and Microanalysis, 2014, 20, 860-861.	0.2	2
265	ALCHEMI Studies of Spinel Oxides for SOFC Interconnect Alloy Coatings. Microscopy and Microanalysis, 2015, 21, 2277-2278.	0.2	2
266	Extended Aging of Ag/W Circuit Breaker Contacts: Influence on Surface Structure, Electrical Properties, and UL Testing Performance. Journal of Materials Engineering and Performance, 2016, 25, 91-101.	1.2	2
267	Microstructural Study of the Heat-treated 17-4PH Stainless Steel Parts Prepared by Selective Laser Melting. Microscopy and Microanalysis, 2017, 23, 2252-2253.	0.2	2
268	Cross Sectional Analysis of Cation Doped Transition Metal Oxide Mesoporous Catalyst Materials. Microscopy and Microanalysis, 2017, 23, 292-293.	0.2	2
269	Studies of the Hierarchical Structure in UCT Manganese Oxides. Microscopy and Microanalysis, 2017, 23, 1864-1865.	0.2	2
270	<i>In Situ</i> Heating to Investigate Phase Transformations in Individual Powder Particles of a Gas-Atomized Icosahedral-Phase-Strengthened Al Alloy. Microscopy and Microanalysis, 2019, 25, 1432-1433.	0.2	2

#	Article	IF	CITATIONS
271	New findings and current controversies in the reaction of ruthenium red and ammonium cerium(iv) nitrate: focus on the precipitated compound. Catalysis Science and Technology, 2020, 10, 2491-2502.	2.1	2
272	Pseudoelasticity of SrNi <sub>2</sub> P <sub>2</sub> Micropillar via Double Lattice Collapse and Expansion. Nano Letters, 2021, 21, 7913-7920.	4.5	2
273	Influence of Substrate Preparation on the Two-Stage MOCVD of CdTe on (001)GaAs. Materials Research Society Symposia Proceedings, 1994, 340, 581.	0.1	1
274	Langmuir-Blodgett Films of Calcium Stearate. Materials Research Society Symposia Proceedings, 1994, 351, 97.	0.1	1
275	An HREM study of the ionic conductor strontium lithium β-alumina. The Philosophical Magazine: Physics of Condensed Matter B, Statistical Mechanics, Electronic, Optical and Magnetic Properties, 1994, 69, 643-654.	0.6	1
276	Identification of the Reference Structure for a High Angle Grain Boundary in Titanium. Materials Science Forum, 1996, 207-209, 289-292.	0.3	1
277	The effect of selected process parameters on laser ablated YBCO thin films on SrTiO3 substrates. Journal of Alloys and Compounds, 1997, 251, 123-128.	2.8	1
278	Analysis of a 69.3° Near-Twist Boundary in Titanium; A Comparison of Two- and Three- Dimensional Models for the Reference Structure. Materials Science Forum, 1998, 294-296, 309-312.	0.3	1
279	The Mechanism of Mixed-Mode Phase Transformations. Materials Research Society Symposia Proceedings, 1999, 586, 21.	0.1	1
280	Analysis of a 69.3° Vicinal HAGB in Pure Titanium. Journal of Materials Science, 2000, 8, 17-25.	1.2	1
281	Nucleation of the C40-to-C11 b transformation in magnetron-sputtered MoSi 2 thin films. Philosophical Magazine Letters, 2002, 82, 687-694.	0.5	1
282	Formation of self-assembled Cu-γ-Al 2 O 3 nanocomposite. Philosophical Magazine Letters, 2003, 83, 135-142.	0.5	1
283	Assembly of CdSe nanocrystals into well-ordered monolayers with a strong crystallographic texture. Philosophical Magazine Letters, 2003, 83, 569-574.	0.5	1
284	Microstructure And Ternary Phases In Al-rich Al-Y-Ni Alloys Materials Research Society Symposia Proceedings, 2003, 806, 208.	0.1	1
285	The Structure of Ribbon Borides in a Ti-44Al-4Nb-4Zr-1B Alloy. Microscopy and Microanalysis, 2005, 11, .	0.2	1
286	Cd2P2Se6 nanolenses formed at a water–air interface. Journal of Materials Science, 2005, 40, 4097-4100.	1.7	1
287	Synthesis and Catalytic Activity of Cryptomelane-Type Manganese Dioxide Nanomaterials Produced by a Novel Solvent-Free Method ChemInform, 2006, 37, no.	0.1	1
288	Devitrification of Al-Y-Ni Glasses. AIP Conference Proceedings, 2008, , .	0.3	1

#	Article	IF	CITATIONS
289	Discontinuous precipitation of β-Ru phase in Ni–18Ru alloys. Journal of Materials Science, 2012, 47, 5701-5705.	1.7	1
290	Characterization of Gadolinium Doped Cerium (IV) Oxides Deposited by Reactive Spray Deposition Technology for Intermediate Temperature Fuel Cell Applications. Microscopy and Microanalysis, 2016, 22, 1344-1345.	0.2	1
291	Electron Microscopy Analysis of 17-4 PH Powder for Additive Manufacturing. Microscopy and Microanalysis, 2016, 22, 1768-1769.	0.2	1
292	In Situ TEM Heating Experiments on PVP-Capped Silver Nano-Cubes. Microscopy and Microanalysis, 2016, 22, 822-823.	0.2	1
293	Fluidized Bed Production of Surface Functionalized Powders for Solid Oxide Fuel Cell Cathodes. ECS Transactions, 2017, 78, 817-825.	0.3	1
294	TEM Specimen Preparation for In Situ Heating Experiments Using FIB. Microscopy and Microanalysis, 2017, 23, 294-295.	0.2	1
295	Effect of Metal-Assisted Catalytic Etching (MACE) on Single-Crystal Si Wafers With Faceted Macropores. Microscopy and Microanalysis, 2019, 25, 2124-2125.	0.2	1
296	Atomic layer adhesion of ferroelectric nanoparticles: a new approach to dielectric composites. Journal of Materials Science, 2020, 55, 16063-16073.	1.7	1
297	Uniaxial compression of [001]-oriented CaFe2As2 single crystals: the effect of microstructure and temperature on superelasticity Part II: Modeling. Acta Materialia, 2021, 203, 116462.	3.8	1
298	In situ electrochemical scanning probe microscopy corrosion studies on duplex stainless steel in aqueous NaCl solutions. Corrosion Engineering Science and Technology, 1996, 31, 139-146.	0.3	1
299	The Formation of Helical Dislocations in Silicon Substrates During Epitaxial Deposition of β- SiC. Materials Research Society Symposia Proceedings, 1989, 162, 445.	0.1	Ο
300	Atomic Force Microscopy of Growth Features on Epitaxial CdHgTe Films. Materials Research Society Symposia Proceedings, 1992, 280, 153.	0.1	0
301	Defect Anisotropy in Movpe CdTe/GaAs. Materials Research Society Symposia Proceedings, 1992, 280, 425.	0.1	Ο
302	The Mechanical Behavior and Deformation Mechanisms of Nb-Al-V Alloys. Materials Research Society Symposia Proceedings, 1996, 460, 671.	0.1	0
303	Instrumental effects on in situ electrochemical STM studies: An investigation of a current surge induced Pd deposit on HOPG. , 1996, 34, 87-95.		Ο
304	Magnetic noise in YBCO thin films and its relationship to growth morphology. IEEE Transactions on Applied Superconductivity, 1997, 7, 1624-1627.	1.1	0
305	Transmission Electron Microscopy Study of YBa2Cu3O7-x Thin Film Multilayer Devices. Materials Research Society Symposia Proceedings, 1997, 474, 107.	0.1	0
306	Mapping the variations in properties of PLD films of YBCO deposited over large areas. Journal of Alloys and Compounds, 1997, 251, 172-175.	2.8	0

#	Article	IF	CITATIONS
307	The Character of Steps on Gamma/Alpha-2 Interfaces in a Low Misfit Lamellar TiAl-Based Alloy. Materials Research Society Symposia Proceedings, 1998, 552, 1.	0.1	0
308	High-Temperature Creep of Nb-Al-V Alloys. Materials Research Society Symposia Proceedings, 1998, 552, 1.	0.1	0
309	The Effect Of Extended Superdislocation / Domain Boundary Interactions in Ordered Intermetallic Compounds. Materials Research Society Symposia Proceedings, 2000, 652, 1.	0.1	0
310	Crystallographic Description for Nanoparticle Asemblies – Application to Cadmium Selenide Clusters. Materials Research Society Symposia Proceedings, 2001, 635, C4.37.1.	0.1	0
311	Synthesis of Metal-doped Cryptomelane Nanomaterials using Cross-linking Reagents. Materials Research Society Symposia Proceedings, 2002, 755, 1.	0.1	0
312	Phase Formation in Ti (Ta)-Ni and Co-Ti Films Deposited on (001)Si in N2 Atmospheres Materials Research Society Symposia Proceedings, 2002, 745, 4101.	0.1	0
313	High-Resolution TEM Characterization of Carbon Aerogels as Catalyst Supports. Materials Research Society Symposia Proceedings, 2003, 800, 348.	0.1	0
314	A Transmission Electron Microscopy Study of Dislocation Substructures in PLD-grown Epitaxial Films of (Ba,Sr)TiO3 on (001) LaAlO3. Materials Research Society Symposia Proceedings, 2003, 784, 271.	0.1	0
315	HREM Studies on the Morphology of CdSe NCs Exposed to Amines. Microscopy and Microanalysis, 2004, 10, 24-25.	0.2	0
316	Structural Transformation Induced by Ion-Milling in TiAl-Based Alloys. Microscopy and Microanalysis, 2004, 10, 700-701.	0.2	0
317	HREM Study of Beta/Gamma Interfaces in a Water-Quenched Ti-44Al-4Nb-4Zr Alloy. Microscopy and Microanalysis, 2004, 10, 288-289.	0.2	0
318	Irradiation-Induced Structural Re-Organization of Carbon Aerogel and Its Derivatives in TEM. Microscopy and Microanalysis, 2005, 11, .	0.2	0
319	Microstructural Studies of a Directionally Solidified Nb-27Mo-27Cr-9Al-9Si Alloy. Microscopy and Microanalysis, 2005, 11, .	0.2	0
320	Control of Nanometer-Scale Tunnel Sizes of Porous Manganese Oxide Octahedral Molecular Sieve Nanomaterials ChemInform, 2005, 36, no.	0.1	0
321	Commensurate Intergrowths in Titanium Monoboride Precipitates. Microscopy and Microanalysis, 2006, 12, 1068-1069.	0.2	0
322	Accommodation of angular incompatibilities between interfacial facets during precipitate growth. Metallurgical and Materials Transactions A: Physical Metallurgy and Materials Science, 2006, 37, 901-909.	1.1	0
323	Stress Relaxation by Cation Ordering in Epitaxial Lead Zirconate Titanate Films. Microscopy and Microanalysis, 2008, 14, 450-451.	0.2	0
324	Plasma Spray of Nano Composite Ceramics Using Solution Precursors and Combustion Synthesized Nano Powders. Materials Research Society Symposia Proceedings, 2009, 1195, 277.	0.1	0

#	Article	IF	CITATIONS
325	Electron Microscopy Resources and Education at the Institute of Materials Science, University of Connecticut. Microscopy and Microanalysis, 2009, 15, 1150-1151.	0.2	Ο
326	Effects of Precursor Chemistry on the Microstructural Characteristics of Sol-Gel/Combustion Synthesized Y2O3-MgO Nano-Composites. Microscopy and Microanalysis, 2010, 16, 1692-1693.	0.2	0
327	Heteroepitaxy: Small 9/2010. Small, 2010, 6, n/a-n/a.	5.2	0
328	Tomographic Reconstruction of Microstructures in Al-Ni-Y-Based Alloys. Microscopy and Microanalysis, 2011, 17, 1856-1857.	0.2	0
329	EPMA Studies on Reactions Between Ti and Al during Spark Plasma Sintering. Microscopy and Microanalysis, 2014, 20, 756-757.	0.2	0
330	Analysis of Titanium Microalloying in As-Received and Oxidized Crofer® 22 APU. Microscopy and Microanalysis, 2014, 20, 892-893.	0.2	0
331	Fractographic Analysis of Co-P-SiC Electrocomposite Coatings by Stereoscopic Reconstruction. Microscopy and Microanalysis, 2014, 20, 1884-1885.	0.2	0
332	Effects of Thermal Processing on Microstructure in P/M Superalloys. Microscopy and Microanalysis, 2016, 22, 1958-1959.	0.2	0
333	TEM Sample Preparation of Ceramic Matrix Composites Using FIB. Microscopy and Microanalysis, 2016, 22, 1836-1837.	0.2	0
334	Microstructural Transformations of La 0.6 Sr 0.4 MnO 3 to nNano-layered Mn Oxide during Electrochemical Water Oxidation. Microscopy and Microanalysis, 2016, 22, 1276-1277.	0.2	0
335	Characterization of Dislocations in Single-Crystalline Ag3Sn Intermetallic Alloys. Microscopy and Microanalysis, 2017, 23, 760-761.	0.2	0
336	Eutectic Solidification in Zn-Sn Binary Alloys: An Experiment for High Schools. Microscopy and Microanalysis, 2017, 23, 2304-2305.	0.2	0
337	SEM Technique Based Automatic Analysis for Metal Powders and Defects in Additive Manufactured Components. Microscopy and Microanalysis, 2018, 24, 652-653.	0.2	0
338	In Situ Phase Transformation of Monodisperse Manganese Oxide Nanoparticles. Microscopy and Microanalysis, 2019, 25, 1896-1897.	0.2	0
339	Localized Corrosion Phenomena in Powder-Processed Icosahedral-Phase-Strengthened Aluminum Alloys. Microscopy and Microanalysis, 2019, 25, 752-753.	0.2	0
340	Effect of Part Placement Strategy on the Microstructure of Additively Manufactured 17-4PH Stainless Steel Thin-Wall Parts. Microscopy and Microanalysis, 2019, 25, 2572-2573.	0.2	0
341	Three-dimensional particle size, shape, and internal porosity characterization: Application to five similar titanium alloy (Ti–6Al–4V) powders and comparison to two-dimensional measurements. Additive Manufacturing, 2021, 44, 102060.	1.7	0
342	Investigation of the laser drilling process by emission spectroscopy. , 2008, , .		0

#	Article	IF	CITATIONS
343	Fluidized Bed Production of Surface Functionalized Powders for Solid Oxide Fuel Cell Cathodes. ECS Meeting Abstracts, 2017, , .	0.0	0
344	Regenerative Electroless Etching of Silicon. ECS Meeting Abstracts, 2017, , .	0.0	0
345	Hierarchical Porous Silicon and Porous Silicon Nanowires Produced with Regenerative Electroless Etching (ReEtching) and Metal Assisted Catalytic Etching (MACE). ECS Meeting Abstracts, 2018, , .	0.0	0
346	Accommodation of angular incompatibilities between interfacial facets during precipitate growth. Metallurgical and Materials Transactions A: Physical Metallurgy and Materials Science, 2006, 37, 901-909.	1.1	0
347	Injection Metal-Assisted Catalytic Etching (MACE) of Si Powder: Discovery of Low-Load MACE and Pore Distribution Tunability Using Ag, Au, Pd, Pt and Cu Catalysts. ECS Meeting Abstracts, 2020, MA2020-02, 1219-1219.	0.0	0